Smart Materials and Structures

PAPER • **OPEN ACCESS**

Vibration energy harvesting from railway tracks via a magnetic–piezoelectric system

To cite this article: Peyman Aela *et al* 2025 *Smart Mater. Struct.* **34** 115030

OPEN ACCESS
IOP Publishing
Smart Materials and Structures
Smart Mater. Struct. **34** (2025) 115030 (16pp)
https://doi.org/10.1088/1361-665X/ae1d39

Vibration energy harvesting from railway tracks via a magnetic–piezoelectric system

Peyman Aela[1], Hung-Lin Chi[2,*], Yiwei Weng[2], Yangsheng Lin[2] and David P Connolly[1]

[1] Institute for High Speed Rail and System Integration, School of Civil Engineering, University of Leeds, Leeds LS2 9JT, United Kingdom
[2] Department of Building and Real Estate, Hong Kong Polytechnic University, Hung Hom, Kowloon, Hong Kong Special Administrative Region of China People's Repubic of China

E-mail: hung-lin.chi@polyu.edu.hk

Received 2 September 2025, revised 24 October 2025
Accepted for publication 7 November 2025
Published 19 November 2025

Abstract

This research addresses the increasing need for renewable energy solutions in the railway transportation sector by proposing a method to convert vibrations into electrical energy. The proposed MagPVDF system uses the coupling of magnetic force and the piezoelectric properties of polyvinylidene fluoride (PVDF) films to harvest vibration energy. The system's structural framework is fabricated using 3D printing with polyethylene terephthalate glycol filament. The design incorporates four PVDF films and four neodymium magnets, creating magnetic levitation that induces PVDF bending and enhances energy generation. Laboratory tests were conducted under cyclic low-frequency loading (4.67–5 Hz) using a mechanical shaker, simulating vibrational conditions with amplitudes comparable to railway track deflections. While sinusoidal loading was used for controlled testing, sensitivity analyses were performed using finite element method simulations, incorporating train-shaped Gaussian load patterns across a broader frequency range (5–30 Hz). Results demonstrated high responsiveness to cyclic loading, with the maximum output voltage (1.4 V per PVDF film) occurring at the resonance frequency (15–20 Hz). These findings highlight the importance of tuning the system for specific vibration frequencies to maximize performance. The MagPVDF system demonstrates potential for sustainable vibrational energy harvesting, making it a promising solution for powering low-energy devices.

Keywords: railway infrastructure, vibration energy harvesting, magnetic levitation, piezoelectric, FEM

1. Introduction

To ensure the safety and reliability of railway infrastructure, real-time condition monitoring is useful for detecting faults before they escalate into significant problems. In recent years, energy harvesting devices have been explored for supporting auxiliary infrastructure on railways, such as powering monitoring sensors and low-energy devices in remote areas [1]. For instance, piezoelectric energy harvesting has shown promise, with studies reporting that under typical traffic loads, a single piezoelectric transducer can achieve a daily energy output of 964 J, highlighting its potential for infrastructure applications [2]. Wireless sensor networks have emerged as a popular solution due to their flexibility and low installation costs [3]. However, a major challenge facing wireless sensor networks is the need for a reliable power source. Conventional

* Author to whom any correspondence should be addressed.

batteries, while common, have limited lifespans and can be difficult to replace or recharge, especially when sensor nodes are distributed over large areas.

In the railway industry, vibration energy harvesting can power wireless sensor networks that monitor track conditions, detect faults, and provide real-time data on train operations [3, 4]. By harnessing kinetic energy that would otherwise be wasted, vibration energy harvesting offers a potentially sustainable and efficient solution for powering low-energy requirement systems [5]. This approach has potential in remote or difficult-to-access areas, such as railway tracks, where regular maintenance and battery replacement are challenging. Additionally, it supports the growing demand for sustainable energy solutions, aligning with global efforts to reduce carbon emissions and dependence on fossil fuels. The potential for energy harvesting from railway track vibrations is significant, prompting investigations into various technologies, including electromagnetic, triboelectric and piezoelectric systems [6–8].

For instance, piezoelectric devices have been successfully deployed on rail sleepers, pavements and bridges, offering low-power solutions for structural health monitoring [9–11]. Electromagnetic harvesters, particularly those employing rotary mechanisms such as ball-screw systems, have shown higher energy outputs and scalability for powering larger sensor networks [12]. Continuous monitoring of track vibrations allows these systems to identify early signs of wear, degradation, or misalignments, enabling timely interventions and reducing the risk of derailments or accidents [13]. Although electromagnetic harvesters offer potential for railway energy harvesting, their deployment faces several challenges. The need for large magnets often increases the overall device volume, reducing power density and making the system less efficient relative to its size. Additionally, the complexity of their design, particularly when optimizing for multiple resonant frequencies or integrating with other systems, can lead to higher manufacturing costs and increased difficulty in maintenance, further limiting their practical application [14]. In contrast, piezoelectric energy harvesters offer advantages such as higher energy density, scalability, and versatility in design [15]. However, many existing piezoelectric systems still struggle to generate sufficient power for practical applications, particularly in environments characterized by high vibration frequencies ranging from 20 to 60 Hz [16], and limited installation space. Recent innovations have introduced nonlinear approaches and compression modes to enhance power output; yet these solutions must also address critical factors like mechanical robustness and the ability to operate effectively within the unique constraints of railway environments [17, 18]. As such, there is a pressing need for the development of compact piezoelectric energy harvesters that can reliably meet these demands while delivering adequate power levels for advanced monitoring systems.

Piezoelectric systems are primarily deployed by the trackside, where they harness the energy generated from the vibrations of trains passing over the tracks [15]. Early work by Nelson *et al* [19] demonstrated the potential of piezoelectric patches mounted on the rail, with predictions indicating that the average power output could increase from field test values to approximately 1.1 mW under loaded train conditions. This initial exploration laid the groundwork for subsequent research into various piezoelectric configurations, including stack-type harvesters, which connect multiple piezoelectric patches mechanically in series and electrically in parallel, achieving mean power outputs of 0.8 mW under optimal conditions [20]. The use of cantilever designs has also been explored, as they can achieve relatively high strain under typical vibration inputs. Gao *et al* [21] proposed a cantilevered piezoelectric vibration energy harvester (PE-VEH) utilizing PZT film, which achieved a maximum power output of 4.9 mW in lab tests. To enhance frequency response, Li *et al* [22] created a piezoelectric transducer with 6 bimorph cantilever beams, achieving a frequency range of 55–75 Hz; however, the maximum power output in field tests was only 0.16 μW, as the excitation frequencies from lower-speed trains fell outside this range. Shan *et al* [23] developed a piezo stack energy harvester, achieving optimal performance at resonant frequencies of 17 Hz and 20 Hz. However, the harvester's performance was highly dependent on external factors such as load resistance and acceleration, leading to potential inconsistencies in power generation, which is a critical consideration for continuous monitoring applications. The compact design, while advantageous for fitting within the confined space of railway tracks, raises concerns about mechanical robustness and long-term durability due to wear from the integrated inertial mass and piezo stack. Despite achieving a maximum average power output of 6.72 mW, this level may be inadequate for more demanding wireless sensor network applications.

One approach is using a mechanical vibration rectifier as proposed by [24, 25] which offers advantages over traditional track vibration energy harvesters. This method minimizes structural alterations to track facilities, improves energy capture from rail vibrations, and enhances design feasibility, processing, and overall lifecycle performance, thus potentially addressing some of the challenges identified in previous research [26, 27]. The proposed system comprises four modules: motion conversion, motion rectification, generator and storage. Experimental results demonstrate that this energy harvester achieves a power output of 28 W. Nonetheless, the high manufacturing and maintenance costs, along with environmental concerns associated with this method, pose barriers to its practical implementation. Based on findings from prior studies [28, 29], at vibration frequencies below 5 Hz, an increase in frequency generally results in higher output voltage and harvested energy. However, at higher frequencies, the results show no consistent pattern, as the peak output voltage varies depending on the test conditions and the type of materials used, with a maximum value observed at a specific load frequency [30, 31].

While previous studies have made significant strides in developing PE-VEHs for railway applications, many existing designs are limited by their narrow operational frequency ranges and power generation efficiencies, sometimes failing

to adapt to the diverse and dynamic vibrational environment of railway systems. Additionally, the integration of piezoelectric systems tends to overlook the potential synergies with magnetic energy harvesting techniques, which could potentially enhance overall energy capture [32, 33]. Thus, this paper combines advanced magnetic–piezoelectric systems, aiming to address these limitations by broadening the operational frequency spectrum and improving energy conversion efficiencies. By leveraging neodymium magnets for levitation and polyvinylidene fluoride (PVDF) films for energy conversion, the study aims to develop a lightweight energy harvester attached below the rail foot that maximizes energy output while minimizing mechanical constraints. This integration seeks to create a more robust and versatile energy harvesting solution, ultimately enhancing the functionality of energy harvesters for railway track superstructures.

2. System design and configuration

The proposed MagPVDF energy harvesting system is designed for installation beneath the rail foot, situated in the space between the sleepers (figure 1). This placement allows the device to harness train-induced vibrations while providing some protection from environmental factors such as rain, sand dunes, and debris compared to locations closer to the railhead. This location also conflicts less with the superstructure kinematic envelope.

In this regard, a magnetic–piezoelectric system was designed using neodymium cylindrical magnets with a diameter of 25 mm and thicknesses of 5 and 10 mm to achieve levitation and enhance the bending of PVDFs. Table 1 presents the specifications of the PVDF films. Inspired by the design of 3D printed energy harvesters for railway bridges by Cámara-Molina *et al* [34, 35], a frame for harvesting rail vibrations was designed using 3D printing of polyethylene terephthalate glycol filament.

As shown in figure 2(a), PVDF films and magnets are housed within a protective cylindrical frame. This enclosure integrates the energy harvesting system with the railway infrastructure while shielding internal components from environmental factors. The frame dimensions were optimized to fit beneath the rail foot in the space between sleepers with an overall height of approximately 80 mm to minimize interference with the superstructure components.

In this study, piezoelectric thin films (PVDF) were selected over more commonly used piezoelectric ceramics due to their flexibility, durability, and ability to withstand the harsh mechanical vibrations typically found in railway environments. Additionally, PVDF films are lightweight and easier to integrate into compact designs, making them ideal for this application. When the inner cylindrical capsule oscillates, the PVDF films mounted on the sides bend, generating electrical energy (figure 2(b)).

The capsule's movement along the shell was facilitated by the magnetic levitation effect, which minimized direct contact and friction between the capsule and the shell wall. This

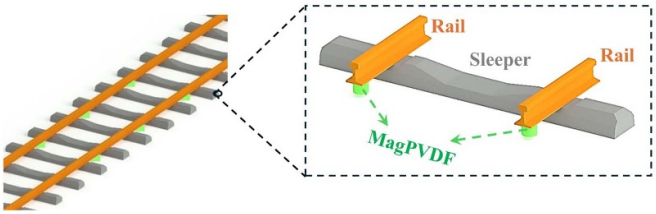

Figure 1. Schematic of proposed energy harvester application.

non-contact mechanism ensured smooth oscillations and prevented significant energy losses due to friction. However, minor frictional forces caused by air resistance or slight misalignments could not be entirely eliminated but were considered negligible in the overall energy conversion process. The 10 mm distance between the magnets was chosen to allow sufficient space for the capsule's oscillatory motion while balancing the magnetic levitation force and the amplitude of oscillations. Two PVDF films were mounted on each side of the capsule to maximize energy harvesting efficiency by ensuring sufficient bending deformation under vibration inputs. This configuration was chosen to balance energy output with structural simplicity while avoiding excessive material usage. The magnetic levitation effect, illustrated in figure 2(c) as magnetic field lines around the installed magnets, increases the bending deformation of the piezoelectric material in response to vibration inputs, thereby boosting energy conversion efficiency. The dimensions of the PVDF thin films were determined based on the available space within the protective frame and the need to achieve optimal bending deformation without mechanical interference. Specifically, the size of 30 mm $\times$ 10 mm was selected to fit the compact cylindrical design while ensuring compatibility with standard railway track dimensions. Notably, this interaction is important for optimizing energy output, while modifying PVDF materials has the potential to further improve their performance for future research [40]. Although increasing the PVDF film size could enhance output power by expanding the effective electrode area (A), thereby elevating voltage and energy through greater capture of magnetic levitation-induced deformations, the MagPVDF device prioritizes compactness for installation under the rail foot between sleepers, avoiding disruption to maintenance such as ballast tamping, rendering larger films impractical due to interference risks.

The electrical output generated by the PVDF elements was measured under varying frequencies and amplitudes. To validate the system's design and configuration, a prototype was subjected to laboratory testing using a shaker device to simulate railway vibrations, with output voltage measured via a digital oscilloscope (appendix B). The experimental procedure begins with activating the vibration source, followed by installing the MagPVDF harvester, applying controlled vibration inputs, measuring voltage and current for performance analysis, and initiating energy harvesting until completion.

Table 1. Track and train parameters [36–39].

Category	Parameter	Value
Train	Train speed (km h^{-1})	200
	Axle load, P_{axle} (N)	108.3
Vehicle	L_c (Wagon length) (m)	22.86
	L_b (Bogie centers) (m)	16
	L_a (Bogie wheelbase) (m)	2.6
	Axle positions (m)	[2.15, 4.75, 18.15, 20.75]
	Number of wagons	24
Track	Rail modulus of elasticity, E_r (Pa)	2.1×10^{11}
	Rail second moment of area, I_r (m^4)	3.04×10^{-6}
	Ballast stiffness, k_b (N m^{-2})	3.15×10^{8}
	Rail pad stiffness, k_p (N m^{-2})	3.5×10^{8}
	Sleeper spacing, L_s (m)	0.6
PVDF	Piezoelectric coefficient d_{31} (pm V^{-1})	23
	Relative permittivity (ϵ_r)	12
	Capacitance (nF)	1.38
	Density (kg m^{-3})	1780
	Young's modulus (Pa)	2×10^{9}
	Electrode area (m^2)	$30 \times 12.2 \times 10^{-6}$
	Length (m)	3×10^{-2}
	Width (m)	1×10^{-2}
	Thickness (m)	28×10^{-6}
Assembly	Length/width/height (mm)	$115 \times 65 \times 75$
Simulation	Track position (m)	25
	Time steps	1000
	Simulation time (s)	10
	Time step size, dt (s)	0.01

This setup confirmed the harvester's ability to generate measurable electrical output from low-frequency vibrations, aligning with the design goals of durability and efficiency in railway environments. The system's performance was validated through prototype laboratory testing, with numerical analysis using finite element method (FEM) ensuring data reliability.

The core of the energy harvester consists of PVDF piezoelectric films. The relationship between mechanical stress (σ), strain (ε), electric field (E), and electric displacement (D) is described by the piezoelectric constitutive equation for a thin beam [41]. The piezoelectric material used in this study is characterized by its ability to couple mechanical and electrical

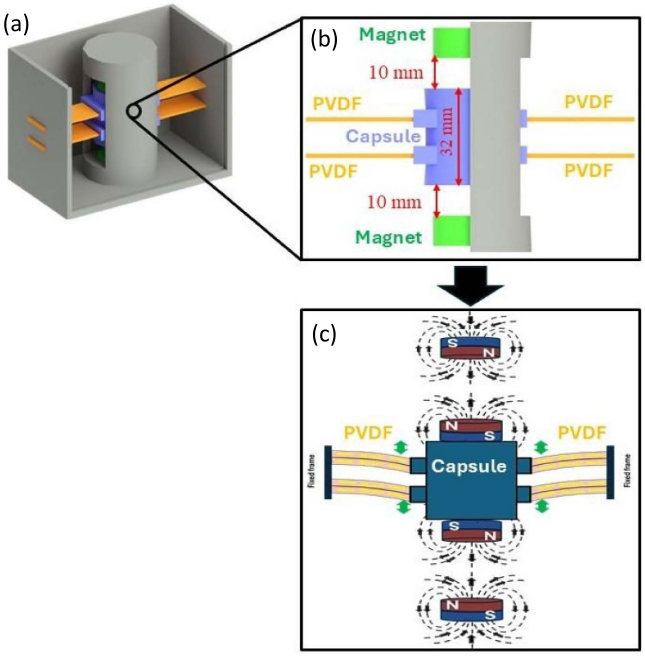

Figure 2. (a) 3D schematic view of the MagPVDF setup, showing the arrangement of the capsule, magnets, and PVDFs, b) cross-sectional structural design of the MagPVDF, illustrating the placement of the magnets and PVDFs with a 10 mm spacing, (c) magnetic field lines generated around the installed magnets, depicting their interactions and alignment with PVDFs.

behaviors. Specifically, the material generates strain (ε_{ij}) in response to an applied electric potential gradient (E_m) and develops an electric potential gradient when subject to mechanical stress (σ_{ij}). This coupling is defined using the piezoelectric strain coefficient matrix (d_{ij}) for unconstrained materials, or the piezoelectric stress coefficient matrix (e_{ij}) for constrained materials. Additionally, the dielectric properties (ϵ_{ij}) of the material describe the relationship between the electric displacement vector (q_i) and the electric field [42]. The governing equation for the piezoelectric material in terms of the piezoelectric strain coefficient matrix (d^{φ}_{mkl}) is expressed in appendix C. There is a relationship between the electric displacement (q_i), the stress (σ_{jk}) and the electric field (E_j). For a thin PVDF beam, this can be simplified to:

$$q_i = d_{31}\sigma + \epsilon E.$$

Given the relative permittivity of $\epsilon_r = 12$ for a PVDF film [43] and permittivity of free space, $\epsilon_0 = 8.854 \times 10^{-12}$ F m^{-1}, the dielectric constant ϵ is 1.062×10^{10} F m^{-1}.

3. Forces acting on the system

3.1. Magnetic dipole–dipole interaction

As shown in figure 2(a), neodymium magnets are strategically positioned to establish a magnetic levitation system around the PVDF films when the device is subject to dynamic train loading. The resulting magnetic force (F_{dipole}) is estimated as [44]:

$$F_{\text{dipole}} = -\frac{3\mu_0 m_1 m_2}{2\pi r^4}$$

where $\mu_0 \approx 4\pi \times 10^{-7}$ N A^{-2} is the permeability of free space [45], m_1 and m_2 are the magnetic dipole moments varying by size of magnets [46], and r is the distance between the magnets. It is assumed that $m = 1.5$ Am^2 is the average value of the magnetic dipole moment of permanent magnets [47], while use of magnets with different size, magnetic moment was defined as $m_1 = 1.5$ and $m_2 = 1$. The restoring force can be linearized by expanding F_{dipole} around an equilibrium distance (r_{eq}), to determine the spring constant, k_{eff}.

3.2. Train-induced rail vibration

This section explores the prediction of vibrations due to moving loads, focusing on the dynamic excitations as described by Thompson [48]. The passage of a train can be modeled as a sequence of traveling loads, where each wheelset applies a force that causes a small deflection of the rail, known as quasi-static deflection. This deflection is dominant at low frequencies, up to 25 Hz for trains moving at 100 km h^{-1}, and up to 100 Hz at 300 km h^{-1} [48]. Ju *et al* [49] provided a method to predict the dominant frequencies during train passage. The dominant frequencies are primarily determined by the ratio between train speed and carriage length and are independent of train speed itself. The influence factor R_f is given by:

$$R_f = |P(f_{\text{dom}})| = \left| \sum_{j=1}^{N_c} \sum_{k=1}^{N_w} P_{\text{axle}} e^{-i2\pi n\left(\frac{s_k}{L_c}+j\right)} \right|$$

where N_c is the number of carriages, N_w is the number of wheel pairs per carriage, P_{axle} is the load per axle, S is the train speed, s_k is the distance between the kth wheel and the beginning of the carriage L_c is the carriage length, and n is an integer multiple representing dominant frequencies. As presented in table 1, our example case is a high-speed train inter-city 125_Mk3 passenger car as investigated by Cleante [36].

To calculate the displacement $\omega(x,t)$ of a railway track subject to a moving static load, we start with the differential equation of motion for a Euler–Bernoulli beam resting on a Winkler foundation, as derived from the analytical models presented by various researchers [48, 50]. The governing equation for a static load P_{axle} acting on the beam can be found in appendix C. By calculating the rail acceleration ($a_{\text{rail}}(x,t) = \frac{\partial^2 w(x,t)}{\partial t^2}$), the maximum recorded acceleration of the sleeper was about 20 m s^{-2}, which matches with the results reported by Cleante [36]. Time history of simulation results for rail deflection/acceleration, and MagPVDF displacement/acceleration can be found in appendix A.

3.3. Electrical output

The energy generated by piezoelectric materials under mechanical stress can be calculated using specific formulations derived from their electrical properties ($E = {}^1/_2\, CV^2$). In piezoelectric materials, the capacitance (C) is a function of piezoelectric charge coefficient (d), dielectric constant (ϵ), electrode area (A), and thickness of the piezoelectric expressed as $C = \frac{\epsilon . A}{h}$. The voltage ($V$) generated in the piezoelectric material is proportional to the applied stress [51]:

$$V = \frac{d_{31} . \Delta\sigma . h}{\epsilon}.$$

Notably, selecting a filler with a greater piezoelectric charge coefficient (d_{31}) and lower dielectric constant (ϵ) is important for harvesting system efficiency.

Given the average track acceleration, $a_{\text{avg}} = 0.03$ m s^{-2}; mass of the MagPVDF capsule, $M_{\text{capsule}} = 0.1$ kg; PVDF length, $L_{\text{PVDF}} = 0.03$ m; width $W_{\text{PVDF}} = 0.0122$ m; and thickness, $H_{\text{PVDF}} = 28 \times 10^{-6}$ m, the induced bending stress on a single PVDF film is $66.4/,$kPa (see appendix C, equations (13)–(15)). Therefore, the output voltage V considering a dielectric constant of $\epsilon = 1.062 \times 10^{-10}$ (F m^{-1}), is 14.38 V. This output voltage is in agreement with the range of reported voltage by previous studies [51, 52]. Notably, the output voltage may not be sufficient for running low-powered sensors in practice due to power loss caused by internal resistance, circuit inefficiencies, and dissipation. Thus, applying rectifiers in a circuit is important for higher effectiveness.

4. Prototype validation

To evaluate the performance of the MagPVDF energy harvesting system, experiments were conducted under low-frequency conditions (5 Hz) using a mechanical shaker. These experiments provided an initial understanding of the system's behavior under controlled conditions. Subsequently, numerical methods were employed to simulate the sinusoidal loading pattern observed in the low-frequency tests. This was followed by applying a train-shaped load pattern to perform a sensitivity analysis of the device performance under higher frequencies corresponding to various train speeds.

4.1. Experimental validation under cyclic loading

The MagPVDF energy harvesting system was tested experimentally using a mechanical shaker to simulate vibrational conditions similar to those found in railway environments. The mechanical shaker, with a working space of 47 × 38 × 17 cm, was used to simulate vibrational conditions and could operate in two modes: orbital and reciprocating [53]. The electrical output generated by the PVDF films was measured using a digital oscilloscope during the oscillatory motion of the magnetic capsule.

The performance of the MagPVDF system was assessed under varying vibration frequencies ranging from 4.67 to 5 Hz, with a nominal shaker displacement of 3 mm. The choice of this narrower band was dictated by the mechanical shaker's operational limit, which could not exceed 5 Hz. However, the actual measured displacement was approximately 2.6 mm due to mechanical constraints of the experimental setup. This

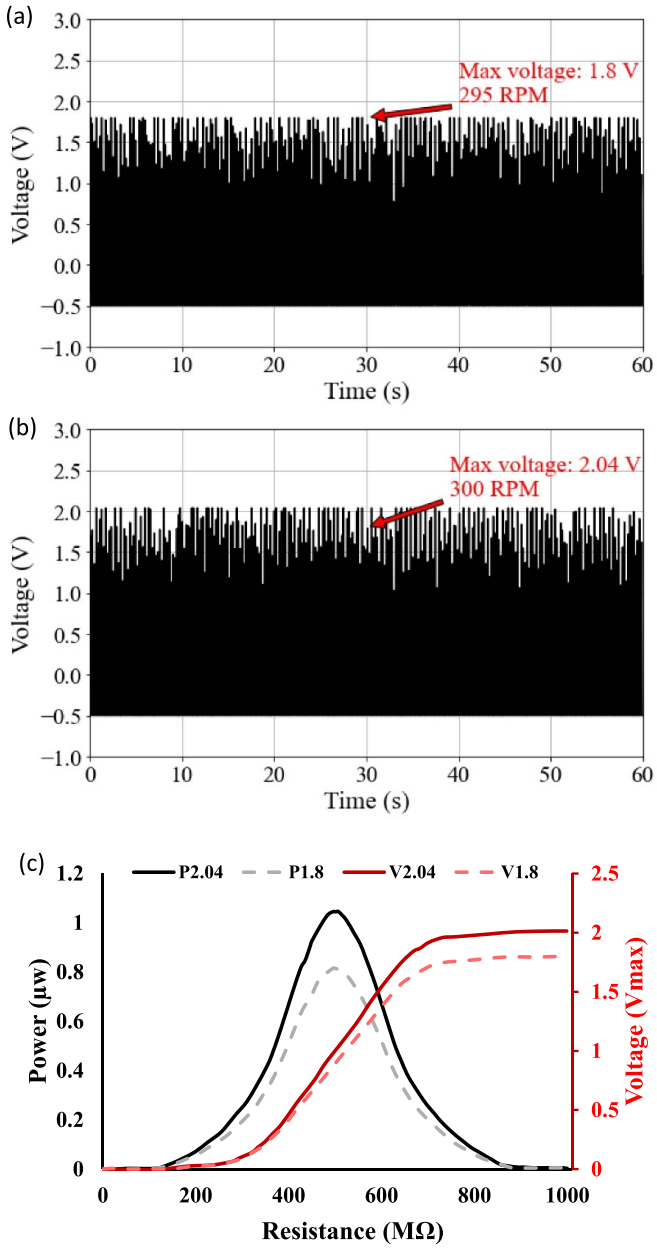

Figure 3. (a) and (b) Sample output voltage for a single PVDF in terms of different vibration frequencies, (c) power output as a function of resistance, highlighting the variation in energy generation efficiency under different conditions.

approach ensured deflections were of similar amplitude to train-induced vibrations. This displacement was further boosted by the magnetic force within the system, enhancing the oscillations of the inner capsule. As the oscillation amplitude of the inner capsule was not directly measured (due to its enclosure within a protective cylinder), it is estimated that the maximum possible movement of the capsule could reach 15 mm, corresponding to the gap between the magnets on the upper and lower sides of the system (figure 2(b)).

The results in figures 3(a) and (b) demonstrated a positive correlation between vibration frequency and energy harvesting performance. At 4.67 Hz (280 RPM), the MagPVDF system produced an output voltage of 1.32 V, which increased to 1.52 V at 4.75 Hz (285 RPM) and further to 1.56 V at 4.83 Hz (290 RPM). At higher frequencies of 5 Hz (300 RPM), the maximum output voltages increased to 2.04 V. The corresponding power output per PVDF film is in the range of 0.8–1.2 μW, totaling 1.2–4.8 μW for the system, comparable to ultra-low-power devices like the BMA400 sensor [54], which operates at ultra-low current levels. The results in figure 3(c) demonstrate the relationship between resistance, output voltage, and generated power for the MagPVDF system. The output voltage (red curve) increases with resistance, eventually stabilizing at a maximum value as resistance minimizes current flow, consistent with the open-circuit behavior of piezoelectric materials [55]. In contrast, the generated power (black curve) exhibits a peak at an optimal resistance (∼542 MΩ), where the trade-off between voltage and current is balanced; at lower resistances, insufficient voltage limits power generation, while at higher resistances, reduced current results in diminished power output. The dashed and solid curves further indicate that higher vibration frequencies broaden and enhance the power peak, as greater mechanical deformation of the PVDF films at higher frequencies generates higher electrical charges. These results underscore the importance of operating the system at its optimal resistance and frequency range to maximize energy output, while also validating the suitability of the PVDF dimensions and configuration for railway-induced vibrations.

Notably, the significant discrepancy between the experimental output and the theoretically calculated voltage in section 3.3 is largely attributed to practical factors, including mechanical damping, material defects, and energy losses within the system. The comparative analysis of voltage and power outputs across tested frequencies confirmed the stable and reliable performance of the MagPVDF system, with the highest energy harvesting capability observed at 5 Hz. These results demonstrate MagPVDF's ability to respond to increasing vibration frequencies by generating higher output voltages, making it a suitable supplemental energy source for low-power railway sensors. However, frequencies beyond 5 Hz were analyzed using FEM, as the maximum frequency attainable by the experimental device was limited to 5 Hz. FEM simulations were employed to evaluate the performance of MagPVDF at higher frequencies relevant to high-speed trains, as discussed in section 4.2.

4.2. Numerical analysis

A FEM analysis was conducted to simulate the behavior of the MagPVDF system under cyclic loading, with a focus on extending the recorded output to higher frequencies (figure 4). Firstly, a single PVDF film was modeled using hexahedra elements with material properties listed in table 1. Specialized piezoelectric elements were used to enable coupling between the mechanical and electrical fields. These elements integrate the mechanical, electrical, and permittivity equations required for simulating piezoelectric behavior. The target global element size was set to approximately 1 mm, ensuring the mesh

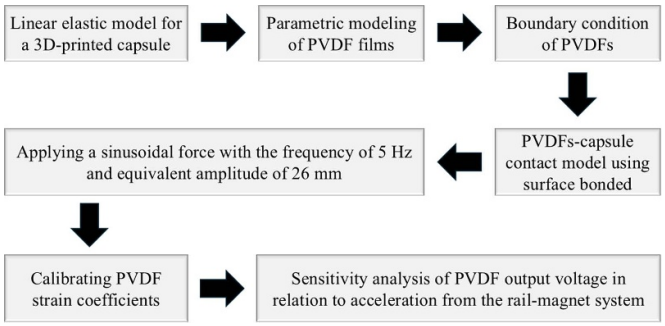

Figure 4. Flowchart of the numerical model steps for MagPVDF system.

could resolve the thin-film geometry and capture stress gradients effectively. Regarding boundary conditions, each PVDF film was modeled with one side fixed while the other side was subject to dynamic loading, replicating its mounting in the experimental setup. The dynamic force applied to the system was a combination of train-induced vibrations and magnetic dipole forces acting on the MagPVDF inner capsule. This approach ensured the model captured the effects of both external vibrations and internal magnetic interactions on the system's performance. The inner capsule itself was modeled as a solid element, and its deformation was neglected to simplify the analysis while focusing on the dynamic response of the PVDF films.

To calibrate the strain coefficients (d_{ij}), a sinusoidal force with a frequency of 5 Hz was applied to simulate the oscillatory motion generated by a shaker device. Figures 5(a) and (b) displays the stress, and output voltage for a single PVDF film in which the highest voltage was observed at the fixed ends of the PVDF film under a sinusoidal load at frequency of 5 Hz. Afterwards, a sensitivity analysis was performed to evaluate the performance of the MagPVDF system at frequencies of 5, 10, 15, 20, and 30 Hz to assess the system's performance across a broader operational range. Figures 5(c) and (d) presents a sample of the measured displacement and output voltage over a 100 s duration under a train-induced load at the frequency of 20 Hz. Magnetic dipole–dipole interactions and the rail vibrations were modeled as the Euler–Bernoulli beam lying on a Winkler foundation with parameters listed in table 1 (appendix A). Thereafter, the applied force on PVDF films during the oscillation of the inner capsule was calculated.

5. Results

5.1. Validation

As shown in figure 6, FEM results for displacement of a single PVDF film exhibited less than 5% deviation. The PVDF strain coefficients (d_{ij}) were calibrated by comparing the FEM results with the experimentally measured output voltage, reaching a maximum value of 1.97 V. The calibrated strain coefficients for the matrix were as follows:

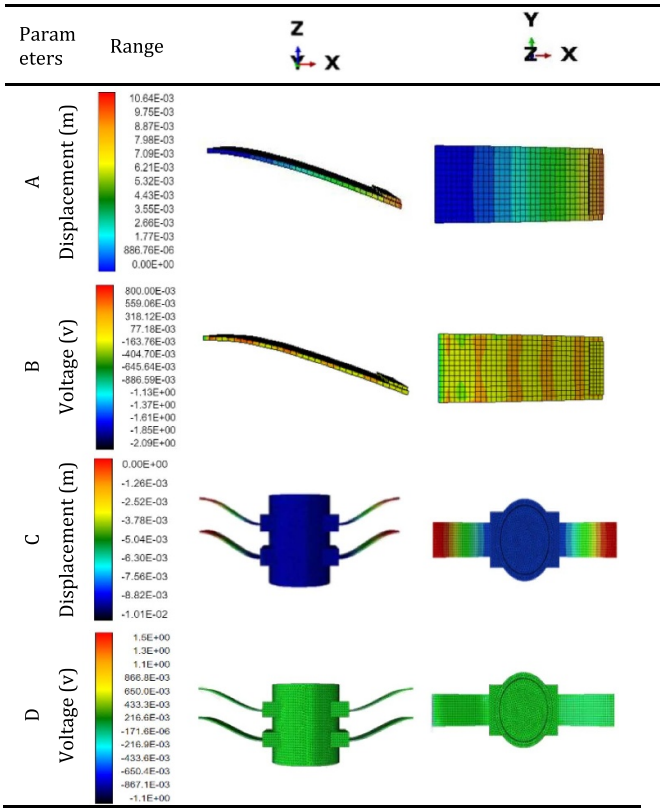

Figure 5. Simulation results for the single PVDF model and MagPVDF model at $F = 20$ Hz: (a) displacement distribution, and (b) output voltage for the single PVDF model, (c) displacement distribution, and (d) output voltage for the MagPVDF model.

$$d^{\varphi}_{1\,11} = d^{\varphi}_{2\,22} = 3.5 \times 10^{-14};$$

$$d^{\varphi}_{1\,22} = d^{\varphi}_{2\,11} = -8.182 \times 10^{-15};$$

$$d^{\varphi}_{1\,33} = d^{\varphi}_{2\,33} = d^{\varphi}_{3\,11} = d^{\varphi}_{3\,22} = -8.124 \times 10^{-15};$$

$$d^{\varphi}_{3\,33} = 4.02 \times 10^{-14}$$

$$d = \begin{bmatrix} d^{\varphi}_{111} & d^{\varphi}_{112} & d^{\varphi}_{113} & 0 & 0 & 0 & 0 & 0 & 0 \\ d^{\varphi}_{121} & d^{\varphi}_{122} & d^{\varphi}_{123} & 0 & 0 & 0 & 0 & 0 & 0 \\ d^{\varphi}_{111} & d^{\varphi}_{132} & d^{\varphi}_{133} & 0 & 0 & 0 & 0 & 0 & 0 \\ 0 & 0 & 0 & d^{\varphi}_{211} & d^{\varphi}_{212} & d^{\varphi}_{213} & 0 & 0 & 0 \\ 0 & 0 & 0 & d^{\varphi}_{221} & d^{\varphi}_{222} & d^{\varphi}_{223} & 0 & 0 & 0 \\ 0 & 0 & 0 & d^{\varphi}_{213} & d^{\varphi}_{232} & d^{\varphi}_{233} & 0 & 0 & 0 \\ 0 & 0 & 0 & 0 & 0 & 0 & d^{\varphi}_{311} & d^{\varphi}_{312} & d^{\varphi}_{313} \\ 0 & 0 & 0 & 0 & 0 & 0 & d^{\varphi}_{321} & d^{\varphi}_{322} & d^{\varphi}_{323} \\ 0 & 0 & 0 & 0 & 0 & 0 & d^{\varphi}_{331} & d^{\varphi}_{332} & d^{\varphi}_{333} \end{bmatrix}.$$

The energy output obtained from the equation of section 3.3, is 4.3 J cm^{-3}, which is in the range of values proposed by Wang *et al* [56].

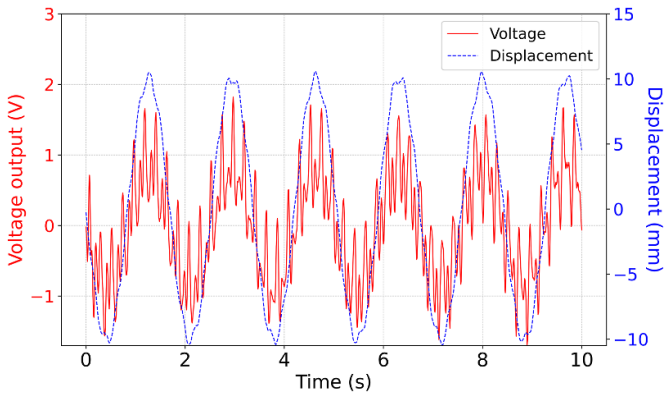

Figure 6. Verification of MagPVDF output voltage under a sinusoidal force.

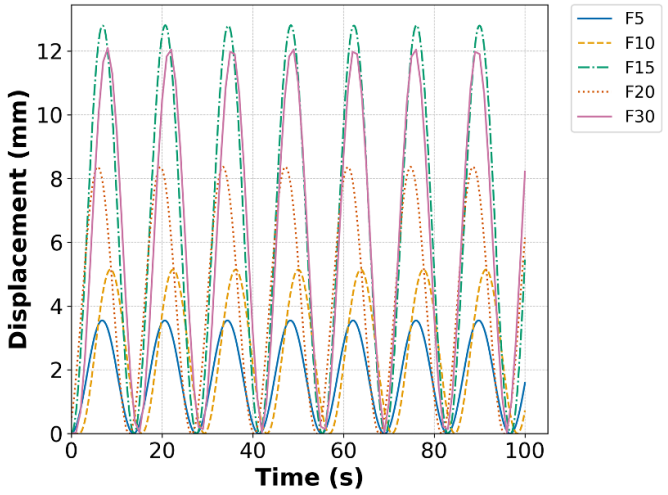

Figure 7. MagPVDF displacement plotted as a function of time for various frequencies (F5, F10, F15, F20, and F30) corresponding to train-load patterns.

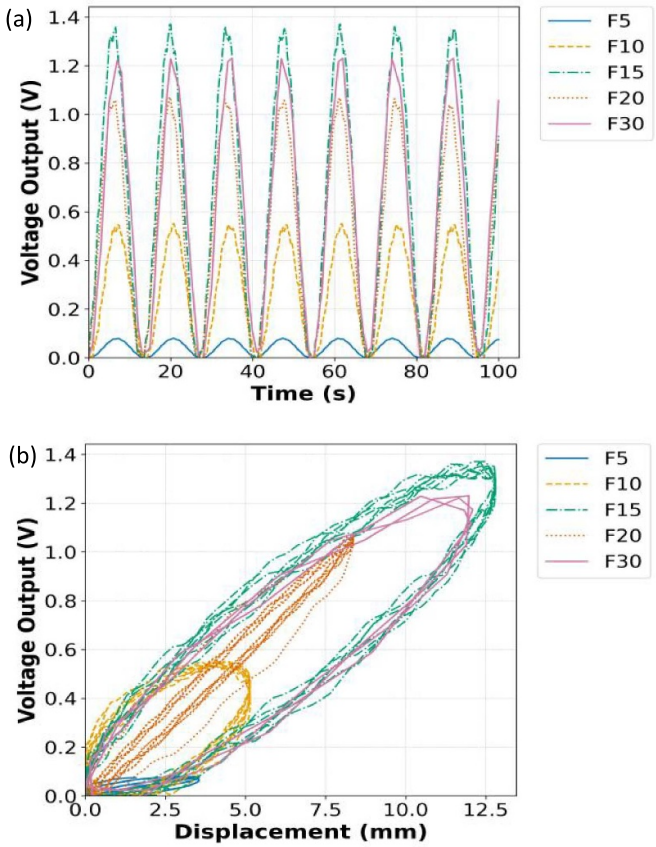

Figure 8. (a) MagPVDF output voltage at different frequencies, (b) voltage–displacement curve.

5.2. Sensitivity analysis

5.2.1. Displacement. Considering the bogie wheelbase, La = 2.6 m, the equivalent train speed was assigned corresponding to the desired frequencies, $f = 5$, 10, 15, 20, and 30 Hz were 46.8, 93.6, 140.4, 187.2, and 280.8 km h^{-1}, respectively. Figure 7 shows the displacement response of the MagPVDF energy harvester under simulated train loading at the above-mentioned frequencies.

The displacement amplitudes exhibit clear frequency-dependent behavior, with the maximum displacement occurring at F15, followed by a slight reduction at F30. At lower frequencies (F5 and F10), the displacement amplitudes are comparatively smaller, indicating reduced mechanical deformation of the MagPVDF harvester. The peak displacement of approximately 12.1 mm at F15 suggests a potential resonance-like behavior, where the harvester's mechanical system responds to the applied train load frequency, maximizing energy harvesting efficiency. The subsequent reduction in displacement at F20 and F30 can be attributed to decreased dynamic responsiveness at higher frequencies. These results highlight the importance of frequency optimization for the MagPVDF energy harvester, show that a 140.4 km h^{-1} train speed provides the most favorable conditions for mechanical deformation and, potentially, electrical energy output.

5.2.2. Output voltage. As shown in figure 8(a), the system demonstrated optimal energy harvesting at 15 Hz, corresponding to a train speed of 140.4 km h^{-1}, where the maximum output voltage was 1.2 V for each single PVDF. At lower frequencies (5–10 Hz), the energy output was significantly lower due to reduced excitation, while at higher frequencies (30 Hz), mechanical damping effects reduced efficiency. Voltage output is directly proportional to strain, which is maximized at resonance, which is close to the resonance frequency reported by Qu *et al* ($F = 13.39$ Hz) [57]. The MagPVDF system is ideal for train speeds ranging from approximately 90–140 km h^{-1}, corresponding to excitation frequencies of 10–15 Hz, which cover the resonance region of the system. This train speed range is common in subway and passenger railway lines, making the system applicable for energy harvesting in these environments.

5.2.3. Efficiency. The magnetic dipole–dipole interactions were found to strongly influence the oscillatory motion of the inner capsule. The forces generated by these interactions were proportional to the square of the magnetic flux density

and were critical in maintaining consistent oscillation amplitudes across the frequency range. At higher frequencies (15–30 Hz), the interactions generated larger restoring forces, amplifying the displacement of the inner capsule and enhancing the energy harvested by the PVDF layer. Figure 8(b) illustrates the voltage–displacement hysteresis behavior of MagPVDF under cyclic loading at different frequencies. The plot shows distinct hysteresis loops for each frequency due to the dielectric permittivity of the PVDF. It implies energy dissipation and nonlinear coupling between mechanical displacement and output voltage as show previously by Panda and Sahoo [58]. As the frequency increases, the loop shape and size change significantly. At $F = 5$ Hz, the loop is narrow and compact, indicating minimal hysteresis and low energy dissipation. At $F = 10$ Hz, the loop is the widest, suggesting the highest energy loss and strong nonlinear effects. At $F = 20$ Hz, the loop is narrower, reflecting lower energy dissipation and a more linear relationship between displacement and voltage. For $F = 15$ Hz, the loop becomes wider, indicating increased hysteresis, possibly due to greater phase lag between voltage and displacement. At F30, however, the loop narrows slightly compared to F15, indicating reduced displacement but still significant energy dissipation. The displacement range also expands with increasing frequency, demonstrating that the system's response is frequency-dependent, possibly close to the natural frequency of the system. The progressive widening of the loops with frequency highlights the dynamic nature of the system and its sensitivity to loading conditions. Overall, the results confirm that frequency significantly impacts the hysteresis behavior, with higher frequencies leading to greater energy dissipation and nonlinear responses. These insights are essential for enhancing material performance in future circuit development and the practical application of MagPVDF.

5.3. Practical implications and limitations

The MagPVDF system demonstrates exceptional potential for ultra-low power applications, similar to the innovative BMA400 acceleration sensor [54]. The BMA400, designed for wearables and smart home devices, uses intelligent power management and consumes as little as 800 nA in ultra-low power mode, with a typical use case of 5.8 μA, ensuring long-lasting battery life. Similarly, the MagPVDF system achieves a maximum open-circuit voltage of approximately 1.4 V per PVDF film and an estimated power output of 2–8 mW for load resistances of 1–10 MΩ, providing sufficient energy to power low-power railway sensors, such as wireless accelerometers or strain gauges. For example, railway sensors typically consume 1–10 μW in sleep mode and 1–5 mW during active data transmission, aligning closely with the MagPVDF system's harvested power [24]. To improve usability, power conditioning circuits are necessary to manage the raw AC output from PVDF films, addressing losses from internal resistance and impedance mismatch [59]. A typical setup includes a full-bridge rectifier for 80%–90% rectification efficiency, and energy storage for buffering [60]. Simulations suggest net usable power of 1–5 mW, suitable for low-power applications. Future work will focus on optimizing impedance matching, interference shielding, and validating durability under real-world conditions.

The experimental validation conducted in this study has certain limitations that must be acknowledged for future research. The experiments were performed under controlled laboratory conditions, which may not fully replicate real-world operational environments. Factors such as temperature variations, external environmental vibrations, and long-term durability were not accounted for and could influence the performance of the system in practical applications. While the prototype demonstrated promising results at the tested scale, its scalability to larger, more complex systems remains uncertain and requires further investigation, particularly for extended operational periods. Lastly, the study primarily focused on a narrow range of vibration frequencies and amplitudes. Broader frequency ranges, as well as multi-axis vibration scenarios, need to be explored in future work to ensure the system's robustness and adaptability to diverse real-world conditions.

6. Conclusion

The MagPVDF system uses the coupling of magnetic force and the piezoelectric properties of PVDF film to harvest vibrational energy. The mechanism relies on the deformation of the PVDF film induced by oscillating magnetic forces, which generates electrical charge due to the piezoelectric effect. This innovative approach enables the conversion of mechanical vibrations into usable electrical energy, making it suitable for low-frequency vibrational environments such as railways.

The close agreement between cyclic loading laboratory tests and FEM results validated the proposed design and simulation methodology against the lab setup. The system exhibited high responsiveness within the frequency range of 5–30 Hz. The results reveal that the maximum output voltage (1.4 V for each PVDF film) occurred at the resonance frequency (15–20 Hz), where the displacement and strain were maximized. At lower frequencies (e.g. 5 Hz), the energy output was reduced due to lower acceleration and force, while at higher frequencies (e.g. 30 Hz), increased damping effects slightly diminished the harvesting efficiency. This behavior highlights the importance of tuning the system to the target vibration frequency range for optimal performance. This tuning can be implemented by adjusting the gap between the magnets and modifying the thickness

of the magnets, which directly influences the system's resonance characteristics. In conclusion, the MagPVDF system demonstrates the potential for vibrational energy harvesting, offering a useful solution for powering low-energy applications.

Data availability statement

The data cannot be made publicly available upon publication because no suitable repository exists for hosting data in this field of study. The data that support the findings of this study are available upon reasonable request from the authors.

Acknowledgment

Gratitude is expressed to the Hong Kong Polytechnic University for the financial support provided (Grant No. P0046657), which has been instrumental in facilitating this research.

Author contributions

Peyman Aela 0000-0001-8798-4644
Conceptualization (lead), Formal analysis (lead), Methodology (lead), Software (lead), Visualization (equal), Writing – original draft (lead)

Hung-Lin Chi
Funding acquisition (lead), Project administration (lead), Resources (supporting), Supervision (lead), Writing – review & editing (supporting)

Yiwei Weng
Resources (supporting), Validation (supporting), Writing – review & editing (supporting)

Yangsheng Lin
Data curation (equal), Investigation (equal), Software (equal)

David P Connolly
Methodology (supporting), Supervision (supporting), Visualization (supporting), Writing – review & editing (equal)

Appendix A

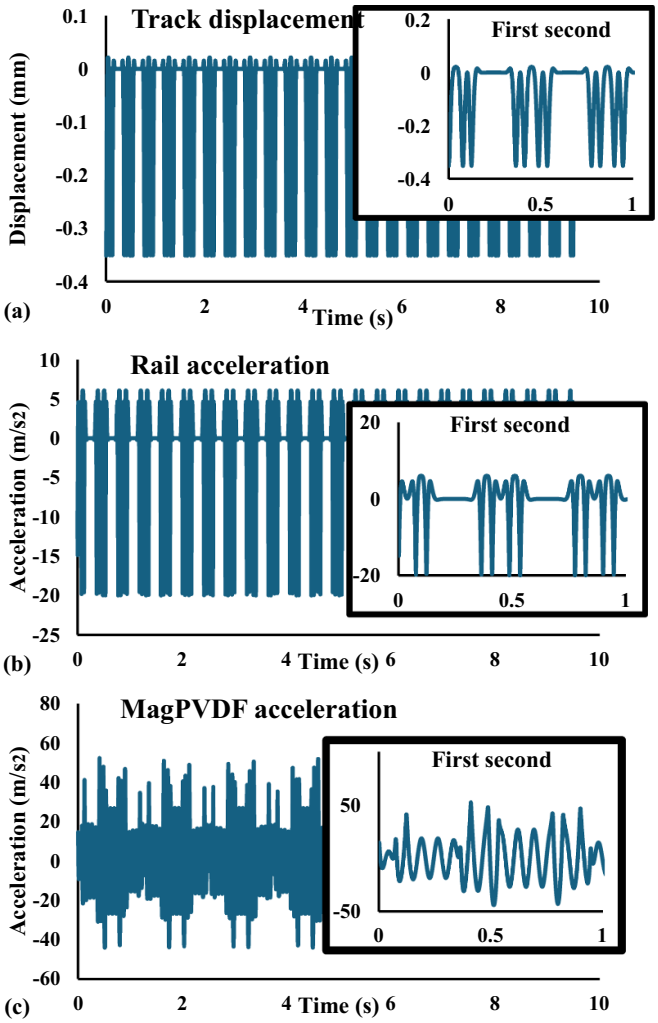

Time history of simulation results for (a) rail deflection, (b) rail acceleration, and (c) MagPVDF acceleration ($m_{\text{capsule}} = 0.1$ kg)

Appendix B

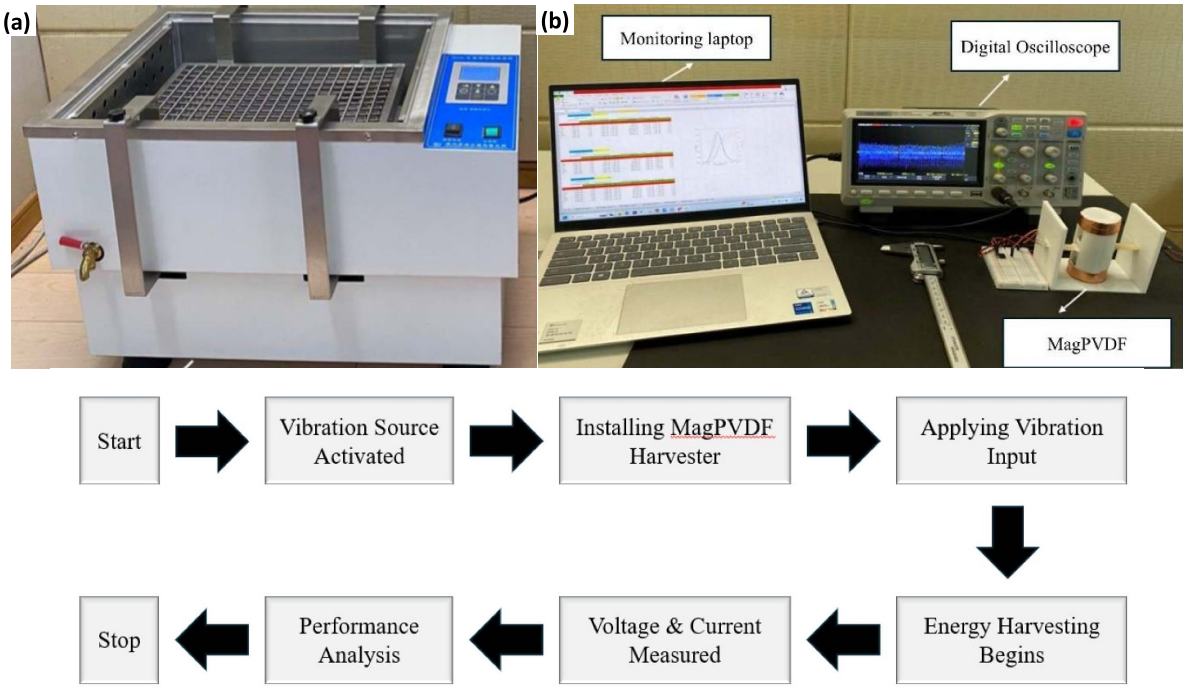

(a) Shaker device, (b) output voltage measurement by oscilloscope, (c) experimental test procedure

Appendix C

Parameters:

$a_{\text{rail}}(x,t)$	Rail acceleration
A	Electrode area
C	Capacitance
d^{φ}_{mkl}	Piezoelectric strain coefficient matrix
d_{31}	Piezoelectric coupling coefficient, relating mechanical stress to electric displacement
D^{E}_{ijkl}	Elastic stiffness matrix at zero electric potential gradient
$D^{\varphi(\sigma)}_{ij}$	Material's dielectric properties
E	Young's modulus of the rail
F_{dipole}	Magnetic restoring force
F_{total}	Total force acting on the MagPVDF system along the z-axis
I	Second moment of area of the rail
k_{f}	Support stiffness per unit length
k_{P}	Stiffness of rail pad per unit length
k_{b}	Stiffness of the ballast per unit length
L_{c}	Carriage length
L_{s}	Sleeper spacing
m_1, m_2	Magnetic dipole moments varying by shape and size of magnets
m_{eff}	Effective mass of the dipole system
n	An integer multiple representing dominant frequencies
N_{c}	Number of carriages
N_{w}	Number of wheel pairs per carriage,
P_{axle}	Load per axle
r	Distance between the magnets
r_{eq}	Equilibrium distance
s_k	Distance between the kth wheel and the beginning of the carriage
s^{E}_{11}	Elastic compliance at constant electric field, relating stress and strain
S	Train speed
V	Voltage across the capacitor
Δz	Rail displacement
$\varepsilon^{\sigma}_{33}$	Permittivity at constant stress, relating electric field to electric displacement
δ	Dirac delta function representing the point load at the position of the wheelset
μ_0	Permeability of free space
ω	Natural frequency of the dipole system

Equations:

$$\begin{bmatrix} \varepsilon_1 \\ D_3 \end{bmatrix} = \begin{bmatrix} s_{11}^E & d_{31} \\ d_{31} & \varepsilon_{33}^\sigma \end{bmatrix} \begin{bmatrix} \sigma_1 \\ E_3 \end{bmatrix} \tag{1}$$

$$\sigma_{ij} = D_{ijkl}^E \left(\varepsilon_{kl} - d_{mkl}^\varphi E_m\right) \tag{2}$$

$$q_i = d_{ijk}^\varphi \sigma_{jk} + D_{ij}^{\varphi\,(\sigma)} E_j \tag{3}$$

$$q_i = d_{31}\sigma + \epsilon E \tag{4}$$

$$\epsilon = \epsilon_{\mathrm{r}}.\epsilon_0 \tag{5}$$

$$F_{\mathrm{dipole}} = -\frac{3\mu_0 m_1 m_2}{2\pi r^4} \tag{6}$$

$$k_{\mathrm{eff}} = \frac{F_{\mathrm{dipole}}(r)}{\Delta r} = -\frac{12\mu_0 m_1 m_2}{2\pi r_{\mathrm{eq}}^5} \tag{7}$$

$$R_{\mathrm{f}} = |P(f_{\mathrm{dom}})| = \left| \sum_{j=1}^{N_{\mathrm{c}}} \sum_{k=1}^{N_{\mathrm{w}}} P_{\mathrm{axle}} \mathrm{e}^{-i2\pi n\left(\frac{x_k}{L_{\mathrm{c}}}+j\right)} \right| \tag{8}$$

$$\mathrm{EI}\frac{\partial^4 w}{\partial x^4} + k_f w = P_{\mathrm{axle}}\delta(x - x_{\mathrm{train}}) \tag{9}$$

$$w(x,t) = \frac{P_{\mathrm{axle}}\beta}{2k_{\mathrm{f}}} \mathrm{e}^{-\beta|x-\mathrm{vt}|} \left(\cos(\beta|x-vt|) + \sin(\beta|x-vt|)\right) \tag{10}$$
$$\beta = \left(\frac{k_{\mathrm{f}}}{4\mathrm{EI}}\right)^{0.25};\ k_{\mathrm{f}} = \left(\frac{1}{k_{\mathrm{p}}} + \frac{1}{k_{\mathrm{b}}}\right)^{-1}/L_{\mathrm{s}}$$

$$F_{\mathrm{total}} = F_{\mathrm{dipole}} - m_{\mathrm{eff}}\, \mathrm{a}_{\mathrm{rail}}(x,t) \tag{11}$$

$$\Delta\ddot{z}(t) + \omega^2 \Delta z = -a_{\mathrm{rail}}(x,t) \tag{12}$$

$$M = F.L = \left(m_{\mathrm{capsule}}.\Delta\ddot{z}(t)_{\mathrm{avg}}\right).L_{\mathrm{PVDF}} \tag{13}$$

$$I = \frac{bh^3}{12} = \frac{0.0122\times\left(1\times10^{-3}\right)}{12} = 1.02\times10^{-12}\mathrm{m}^4 \tag{14}$$

$$\sigma = \frac{M.y}{I} = \frac{9\times10^{-5}\times0.75\times10^{-3}}{1.02\times10^{-12}} = 66.4\,\mathrm{kPa} \tag{15}$$

$$V = \frac{d_{31},\Delta\sigma.h}{\epsilon} \tag{16}$$

$$E = \frac{d_{31}^2}{2\epsilon} A.h.(\Delta\sigma)^2 \tag{17}$$

References

[1] Pourghodrat A, Nelson C A, Hansen S E, Kamarajugadda V and Platt S R 2014 Power harvesting systems design for railroad safety *Proc. Inst. Mech. Eng. F* **228** 504–21

[2] Cao Y, Sha A, Liu Z, Li J and Jiang W 2021 Energy output of piezoelectric transducers and pavements under simulated traffic load *J. Clean. Prod.* **279** 123508

[3] Hodge V J, Keefe S O, Weeks M and Moulds A 2015 Wireless sensor networks for condition monitoring in the railway industry: a survey *IEEE Trans. Intell. Transp. Syst.* **16** 1088–106

[4] Min Z, Du X, Zhang X, Wu W, Shan X and Xie T 2024 Picking up railway track vibration energy using a novel doughnut-shaped piezoelectric energy harvester *Energy* **310** 133183

[5] Lacerda I S, Silva A A, Fernandes E M, Senko R, Oliveira A G, Delgado J M P Q, Diniz D D S, Figueiredo M J and Lima A G B 2024 Comparative analysis of piezoelectric transducers for low-power systems: a focus on vibration energy harvesting *Appl. Sci.* **14** 9451

[6] Zhang H, Su X, Quan L, Jiang J, Dong B and Wei G 2021 Sponge-supported triboelectric nanogenerator for energy harvesting from rail vibration *J. Energy Eng.* **147** 04021006

[7] Zhang T, Kong L, Zhu Z, Wu X, Li H, Zhang Z and Yan J 2024 An electromagnetic vibration energy harvesting system based on series coupling input mechanism for freight railroads *Appl. Energy* **353** 122047

[8] Pei J, Guo F, Zhang J, Zhou B, Bi Y and Li R 2021 Review and analysis of energy harvesting technologies in roadway transportation *J. Clean. Prod.* **288** 125338

[9] Min Z, Sui G, Hou C, Zhang X, Shan X and Xie T 2024 Study on energy capture characteristics of piezoelectric stack energy harvester for railway track *AIP Adv.* **14** 045311

[10] Sheng W, Xiang H, Zhang Z and Wang J 2025 Experimental study and application of a self-powered wireless health monitoring system for railway bridges based on piezoelectric energy harvesting *Energy* **317** 134583

[11] Cao Y, Li J, Sha A, Liu Z, Zhang F and Li X 2022 A power-intensive piezoelectric energy harvester with efficient load utilization for road energy collection: design, testing, and application *J. Clean. Prod.* **369** 133287

[12] Wang T, Lv H and Wang X 2024 Development of an electromagnetic energy harvester for ultra-low frequency pitch vibration of unmanned marine devices *Appl. Energy* **353** 122072

[13] Sun W, Thompson D J, Yurchenko D, Zhao D, Luo Z and Khan I 2025 Energy harvesting technologies on high-speed railway infrastructure: review and comparative analysis of the potential and practicality *Sustain. Energy Technol. Assess.* **74** 104187

[14] Muscat A, Bhattacharya S and Zhu Y 2022 Electromagnetic vibrational energy harvesters: a review *Sensors* **22** 5555

[15] Zuo J, Dong L, Yang F, Guo Z, Wang T and Zuo L 2023 Energy harvesting solutions for railway transportation: a comprehensive review *Renew. Energy* **202** 56–87

[16] Zhai W, Wei K, Song X and Shao M 2015 Experimental investigation into ground vibrations induced by very high speed trains on a non-ballasted track *Soil Dyn. Earthq. Eng.* **72** 24–36

[17] Domínguez-Pumar M, Pons-Nin J, Chávez-Domínguez J A 2016 *Nonlinearity in Energy Harvesting Systems: Micro- and Nanoscale Applications* ed E Blokhina *et al* (Springer) pp 23–63

[18] Cheng Q, Wang Q, Liu Z and Lv Z 2024 Theoretical and experiment optimization research of a frequency up-converted piezoelectric energy harvester based on impact and magnetic force *Eng. Res. Exp.* **6** 035314

[19] Nelson C A, Platt S R, Albrecht D, Kamarajugadda V and Fateh M 2008 Power harvesting for railroad track health monitoring using piezoelectric and inductive devices *Proc. SPIE* **6928** 69280R

[20] Wang J, Shi Z, Xiang H and Song G 2015 Modeling on energy harvesting from a railway system using piezoelectric transducers *Smart Mater. Struct.* **24** 105017

[21] Gao M, Wang P, Cao Y, Chen R and Liu C 2016 A rail-borne piezoelectric transducer for energy harvesting of railway vibration *J. Vib. Eng.* **18** 4647–63

[22] Li J, Jang S and Tang J 2014 Implementation of a piezoelectric energy harvester in railway health monitoring *Proc. SPIE* **9061** 90612Q

[23] Shan G, Kuang Y and Zhu M 2022 Design, modelling and testing of a compact piezoelectric transducer for railway track vibration energy harvesting *Sens. Actuators A* **347** 113980

[24] Liu G, Fang Z, Zhang Z, Tan X, Dai C, Wu X, Jin Z and Li D 2022 A vibration energy harvester for freight train track self-powered application *iScience* **25** 105155

[25] Zhang X, Pan H, Qi L, Zhang Z, Yuan Y and Liu Y 2017 A renewable energy harvesting system using a mechanical vibration rectifier (MVR) for railroads *Appl. Energy* **204** 1535–43

[26] Kim S-C, Kim J-G, Kim Y-C, Yang S-J and Lee H 2019 A study of electromagnetic vibration energy harvesters: design optimization and experimental validation *Int. J. Precis. Eng. Manuf. Green Technol.* **6** 779–88

[27] Jin J-W, Kang K-W and Kim J-H 2015 Development of durability test procedure of vibration-based energy harvester in railway vehicle *Int. J. Precis. Eng. Manuf. Green Technol.* **2** 353–8

[28] Li S, Ren D, Guo P, Wang H, Xu B and Jiang N 2024 Energy harvesting from low-frequency vibrations of hanger using PVDF: an experimental study and performance analysis *Energy* **291** 130427

[29] Kang J, Liu T, Lu Y, Lu L, Dong K, Wang S, Li B, Yao Y, Bai Y and Fan W 2022 Polyvinylidene fluoride piezoelectric yarn for real-time damage monitoring of advanced 3D textile composites *Composites B* **245** 110229

[30] Koç M 2024 Effect of multilayer fabrication of PVDF/PZT fibers on output performance in piezoelectric nanogenerator (PEN) *J. Polym. Res.* **31** 160

[31] Ghafari E, Nantung T and Lu N 2019 An efficient polyvinylidene fluoride (PVDF) nanogenerator for energy harvesting in low frequency range *ES Mater. Manuf.* **5** 72–77

[32] Zhang X, Li G and Su S 2024 Numerical and experimental performance study of magnetic levitation energy harvester with magnetic liquid for low-power-device's energy storage *J. Energy Storage* **75** 109584

[33] Wang L, Zhang Y, Liu S, Zhao L-C, Hu K-M, Li Z, Zhao L, Zhang W-M and Meng G 2025 Enhanced vibration energy harvesting of magnetically coupled piezoelectric cantilever beam with double-point stopper *Mech. Syst. Signal Process.* **233** 112791

[34] Cámara-Molina J C, Romero A, Moliner E, Connolly D P, Martínez-Rodrigo M D, Yurchenko D and Galvín P 2024 Design, tuning and in-field validation of energy harvesters for railway bridges *Mech. Syst. Signal Process.* **208** 111012

[35] Cámara-Molina J C, Moliner E, Martínez-Rodrigo M D, Connolly D P, Yurchenko D, Galvín P and Romero A 2023 3D printed energy harvesters for railway bridges-design optimisation *Mech. Syst. Signal Process.* **190** 110133

[36] Cleante V G 2015 Effects of railway track vibration induced by passing trains on an energy harvesting device (Universidade Estadual Paulista Júlio de Mesquita Filho, Faculdade de Engenharia)

[37] K&J Magnetics I 2024 Neodymium magnet specifications
[38] Dallaev R, Pisarenko T, Sobola D, Orudzhev F, Ramazanov S and Trčka T 2022 Brief review of PVDF properties and applications potential *Polymers* **14** 4793
[39] Fotouhi S, Akrami R, Ferreira-Green K, Naser G A M, Fotouhi M and Fragassa C 2019 Piezoelectric PVDF sensor as a reliable device for strain/load monitoring of engineering structures *IOP Conf. Ser.: Mater. Sci. Eng.* **659** 012085
[40] Ramana E V, Durairajan A, Kavitha D, Tobaldi D M, Zavašnik J, Bdikin I and Valente M A 2024 Enhanced magnetoelectric and energy storage performance of strain-modified PVDF-$Ba_{0.7}Ca_{0.3}TiO_3$-$Co_{0.6}Zn_{0.4}Fe_2O_4$ nanocomposites *J. Energy Storage* **87** 111454
[41] Erturk A and Inman D 2011 *Piezoelectric Energy Harvesting* (Wiley) pp 1–18
[42] Smith M 2009 ABAQUS/standard user's manual, version 6.9. (Dassault Systèmes Simulia Corp)
[43] Isarakorn D, Sambri A, Janphuang P, Briand D, Gariglio S, Triscone J, Guy F, Reiner J, Ahn C and De Rooij N 2010 Epitaxial piezoelectric MEMS on silicon *J. Micromech. Microeng.* **20** 055008
[44] Castañer R, Medina J M and Cuesta-Bolao M J 2006 The magnetic dipole interaction as measured by spring dynamometers *Am. J. Phys.* **74** 510–3
[45] Education E 2024 Permeability of free space (University of Calgary)
[46] Whites K W 2005 *The Electrical Engineering Handbook* ed W-K Chen (Academic) pp 479–97
[47] Amrani D 2015 Determination of magnetic dipole moment of permanent disc magnet with two different methods *Phys. Educ.* **31** 1–6 (available at: www.physedu.in/publication/search/18/279)
[48] Thompson D 2009 *Railway Noise and Vibration* ed D Thompson (Elsevier) pp 29–95
[49] Ju S-H, Lin H-T and Huang J-Y 2009 Dominant frequencies of train-induced vibrations *J. Sound Vib.* **319** 247–59
[50] Grassie S L, Gregory R W, Harrison D and Johnson K L 1982 The dynamic response of railway track to high frequency vertical excitation *J. Mech. Eng. Sci.* **24** 77–90
[51] Fu J, Hou Y, Gao X, Zheng M and Zhu M 2018 Highly durable piezoelectric energy harvester based on a PVDF flexible nanocomposite filled with oriented $BaTi_2O_5$ nanorods with high power density *Nano Energy* **52** 391–401
[52] Jiang Y, Deng Y and Qi H 2021 Microstructure dependence of output performance in flexible PVDF piezoelectric nanogenerators *Polymers* **13** 3252
[53] LABO-HUB 2024 Thermostatic water bath shaker
[54] BOSCH 2024 *Ultra-low Power Accelerometer BMA400 from Bosch for IoT and Wearables Available through Distribution* (Bosch Sensortec GmbH)
[55] Kim S-G, Priya S and Kanno I 2012 Piezoelectric MEMS for energy harvesting *MRS Bull.* **37** 1039–50
[56] Wang H, Xie H, Wang S, Gao Z, Li C, Hu G-H and Xiong C 2018 Enhanced dielectric property and energy storage density of PVDF-HFP based dielectric composites by incorporation of silver nanoparticles-decorated exfoliated montmorillonite nanoplatelets *Composites A* **108** 62–68
[57] Qu S, Ren Y, Hu G, Ding W, Dong L, Yang J, Wu Z, Zhu S, Yang Y and Zhai W 2024 Event-driven piezoelectric energy harvesting for railway field applications *Appl. Energy* **364** 123160
[58] Panda P K and Sahoo B 2015 PZT to lead free piezo ceramics: a review *Ferroelectrics* **474** 128–43
[59] Savarimuthu K, Sankararajan R and Murugesan S 2017 Analysis and design of power conditioning circuit for piezoelectric vibration energy harvester *IET Sci. Meas. Technol.* **11** 723–30
[60] Peng Y, Choo K D, Oh S, Lee I, Jang T, Kim Y, Lim J, Blaauw D and Sylvester D 2019 An efficient piezoelectric energy harvesting interface circuit using a sense-and-set rectifier *IEEE J. Solid-State Circuits* **54** 3348–61